JMEPEG (2008) 17:586–593
DOI: 10.1007/s11665-007-9184-2

1059-9495/$19.00

Assessment of the Effect of Microstructure on the Magnetic Behavior of Structural Carbon Steels Using an Electromagnetic Sensor

F. Rumiche, J.E. Indacochea, and M.L. Wang

(Submitted September 7, 2007)

The magnetic properties of four carbon steels were evaluated using an electromagnetic sensor and correlated with their microstructures. Their composition, microstructure features (such as ferrite volume fraction, grain size, inclusions, etc), and hardness were compared with their saturated magnetic flux density, retentivity, and coercivity. The four steel rods used in this study were hot-rolled AISI 1010, AISI 1018, AISI 1045, and AISI 1045-high manganese/"stress proof." The results show that microstructures have a notable effect on the magnetic properties of the steels. In addition, the effect of variations in cross-section area of the steel rods on the magnetic response was investigated. The steel rods diameters were systematically reduced by machining and then magnetically evaluated. Consistent relationships between metallurgical characteristics of the structural carbon steels and their magnetic properties measured with the electromagnetic sensor were obtained. In addition, the sensor was found to be able to detect changes in magnetic properties due to variations in cross-section area. These results reveal that the electromagnetic sensor has the potential to be used as a reliable nondestructive tool to detect and monitor microstructural and morphological changes occurring during the different stages of steel manufacturing or alterations caused by a degradation mechanism.

Keywords electromagnetic sensor, magnetic properties, structural steel

1. Introduction

An adequate process control during manufacturing of steels is crucial to maintaining microstructural homogeneity and consistency in mechanical properties. In the case of hot-rolled steel it is important to control variations in temperature distribution and rates during cooling that can affect final microstructures. Similarly, in high-strength steels the development of second phases needs to be monitored during cooling to obtain the desired mechanical properties. On the other hand, the magnetic properties of ferromagnetic materials are influenced by their chemical composition and microstructure. It is then feasible to follow the microstructural variations in steels during manufacturing processing or their degradation by measuring and monitoring changes in magnetic properties.

Several magnetic-based systems have been developed to monitor steel processing. Mesina et al. (Ref 1) designed a pulsed electromagnetic sensor for automatic sorting of scrap stainless steel. Haldane and Papaelias et al. (Ref 2, 3) developed a multifrequency sensor for the measurement of ferrite/austenite phase fraction and identification of phase transformation during the production of strip steel with dual or multiphase microstructures. Mohri et al. (Ref 4) presented micromagnetic sensors for the evaluation of pinholes and defects in steel sheets and rods. Taylor (Ref 5) used electromagnetic sensors to measure the grain size of continuous moving steel sheet at various stages of processing.

Degauque et al. (Ref 6) reported that the magnetic domain size is proportional to the square root of grain size for grain diameters between 0.05 and 1.0 mm; magnetic properties are affected by the grain size because of the generation of closure domains at the grain boundaries, which provide obstacles to the movement of the domain walls during magnetization. Angladа-Rivera et al. (Ref 7) studied the effect of grain size on the hysteresis loop in commercial 1005 carbon steel (C-0.04; Mn-0.82 P-0.016; S-0.027); different specimens of this steel were submitted to different heat treatments to produce several grain sizes as observed in Table 1 and shown in Fig. 1. They found changes in the hysteresis curves as a result of variations in grain size; they also determined that the induced magnetic saturation or B_{max} decreased with grain size coarsening (Fig. 2).

Tanner et al. (Ref 8) observed a linear trend between coercivity H_c and the inverse of the grain size and they also correlated H_c to the presence of ferrite and pearlite according to the equation:

$$H_c = c_1\left(\frac{V_p}{d_p}\right) + c_2\left(\frac{V_f}{d_f}\right) \quad \text{(Eq 1)}$$

where V_p and V_f are the pearlite and ferrite volume fractions, and d_p and d_f are the pearlite colony size and ferrite grain size, respectively; c_1 and c_2 are constants. In general, they established that any additional microstructural constituent in carbon steels (i.e., pearlite in a ferritic matrix) tends to dominate the magnetic behavior when it is present in ample

F. Rumiche, J.E. Indacochea, and **M.L. Wang**, Department of Civil and Materials Engineering, University of Illinois at Chicago, 842 W. Taylor St., Chicago, IL 60607. Contact e-mail: jeindaco@uic.edu.

Table 1 Heat treatments and grain sizes in this study (Ref 7)

Heat treatment procedure	Grain size, μm
Austenitized at 900 °C, 1 h; air cool to room temperature	20
Austenitized at 900 °C, 1 h; furnace cool to 650 °C; then air cool to room temperature	35
Austenitized at 900 °C, 1 h; furnace cool to room temperature	45

quantities. Yoshino et al. (Ref 9) also stated that pearlite does not significantly affect H_c at volume fractions less than 17%. Furthermore, when pearlite constitutes more than the 60% of the microstructure, H_c increases proportionally to the pearlite fraction independently of the grain size. In the same way, H_c is dominated by the martensite percent rather than the ferrite grain size in ferritic steels containing more than 15% of martensite. For austenitized, quenched, and tempered plain-carbon steels, the prior austenite grain size has a negligible effect on the hysteresis loop characteristics.

Our study uses an electromagnetic sensor developed at the University of Illinois at Chicago (Ref 10-13) to evaluate structural carbon steels microstructures by measuring their magnetic properties. Furthermore, since most of the materials degradation mechanisms, such as corrosion, creep, and fatigue, change the area of the affected component, the feasibility of using the electromagnetic sensor to detect changes in cross-section area of steels was evaluated.

2. Experimental Details

2.1 Materials and Experimental Approach

Cylindrical rods 12.5 mm in diameter and 813 mm long of four different structural steels, hot-rolled AISI 1010, AISI 1018, AISI 1045, and AISI 1045-high manganese/stress-proof, were used in this study. Their chemical composition and corresponding microstructures are presented in Table 2 and Fig. 3. The magnetic response of the samples was recorded using an electromagnetic (EM) sensor. Before magnetization and generation of the hysteresis curves for each specimen, the samples were demagnetized. The parameters for a hysteresis cycle were: ±10 A demagnetizing current; 100 s demagnetizing time, 1 Hz demagnetizing frequency, and ±10 A hysteresis current. The curves were plotted in SI units of Tesla (T) for the magnetic induction and amperes per meter (A/m) for the magnetic field H. Three measurements were performed per sample and the data was statistically analyzed. All measurements were conducted at room temperature. The measured magnetic properties were then correlated with steel metallurgical features such as carbon content, ferrite volume fraction, grain size, and hardness.

The specimen diameters were reduced by machining at the rod mid-length in a zone 50.8 mm long, in the amounts of 5, 10, and 15%, for each steel. Figure 4 depicts the machined AISI 1045 steel samples. The magnetic flux density was recorded in each case and correlated with the degree of mass loss due to reduction in cross-sectional area.

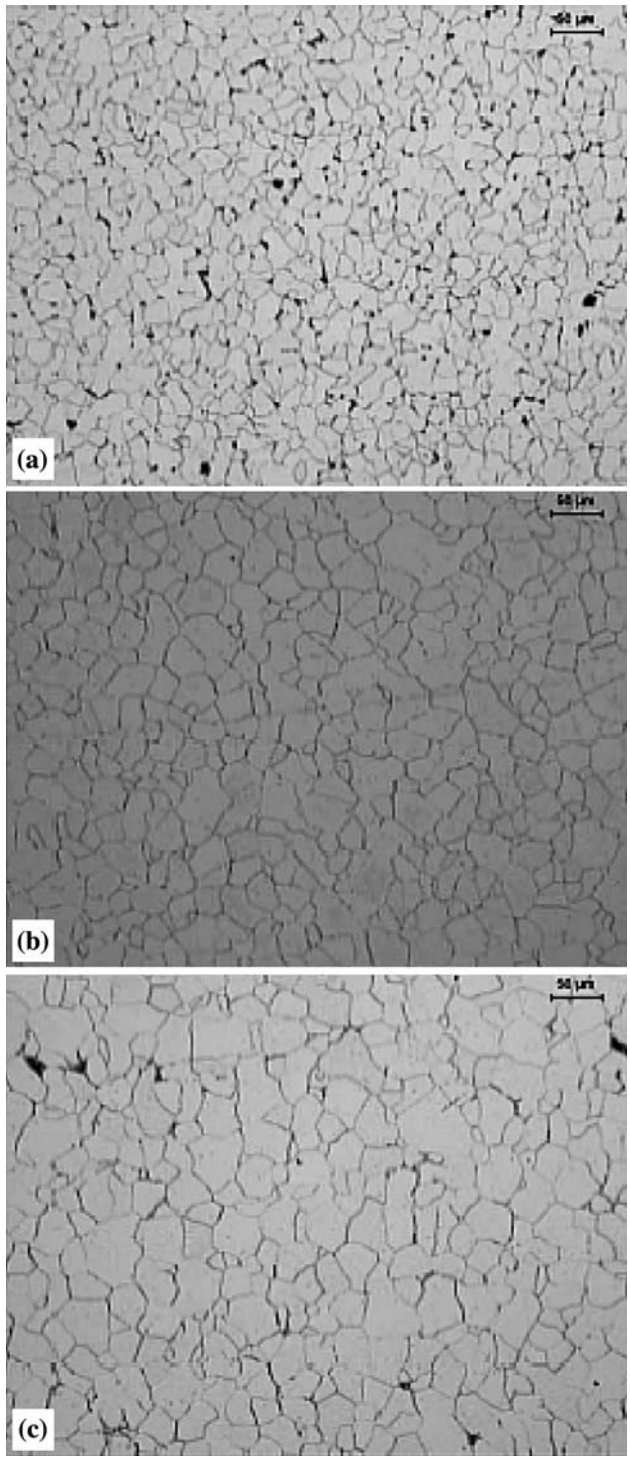

Fig. 1 Optical micrographs displaying the different grain sizes of specimens considered in the investigation (Ref 7): (a) 20 μm, (b) 35 μm, and (c) 45 μm

2.2 Description of the EM Sensor

The EM sensor and measuring system consisted of a primary coil or solenoid that magnetizes the steel samples; the secondary coil wound on the test sample senses changes of magnetic flux. There is a voltage induced by these flux changes which is processed by an electronic integrator, which takes into consideration a fixed cross-section area of the 12.5 mm

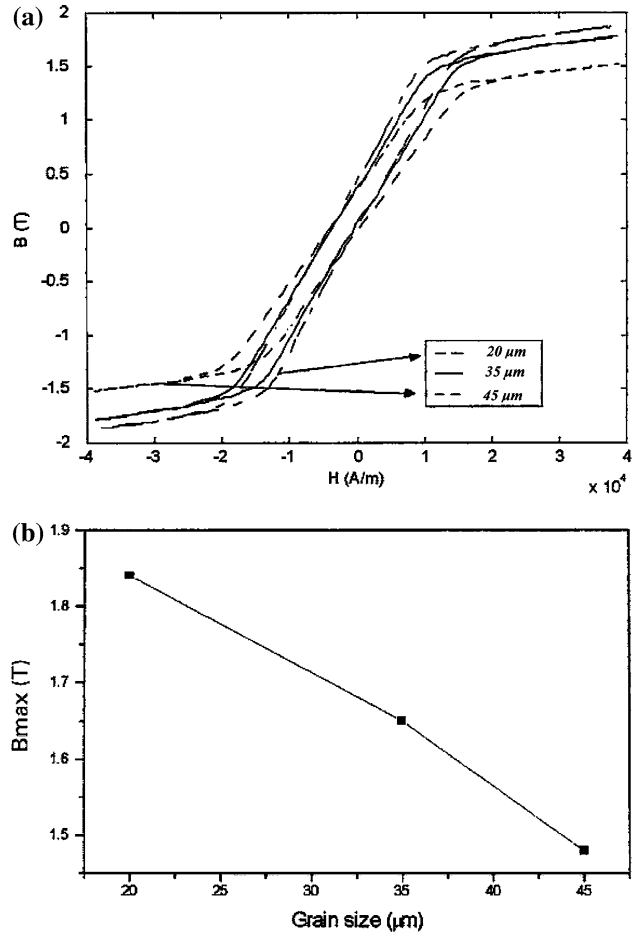

Fig. 2 (a) Effect of grain size on the magnetic hysteresis curve of AISI 1005 steel. (b) Variation of B_{max} with grain size in the same steel (Ref 7)

Table 2 Chemical composition of steels studied

	Element, wt.%				
Steel	**C**	**Mn**	**P**	**S**	**Si**
AISI 1010-hot-rolled	0.11	0.65	0.012	0.027	0.18
AISI 1018	0.17	0.77	0.012	0.030	0.19
AISI 1045	0.52	0.83	0.008	0.013	0.27
AISI 1045-High Mn/stress-proof	0.48	1.57	0.009	0.040	0.20

diameter rod (122.7 mm^2). The secondary coil is placed concentrically with the primary coil. The tangential component of the intensity of the magnetic field is measured by an array of Hall sensors conveniently located close to the surface of the specimen. Figure 5 shows the details of the EM sensor. The Hall sensors were initially calibrated to relate reliably the magnetic intensity to the output voltage. The array of Hall sensors can be treated as a line arrangement, provided that the configuration is placed in a magnetic field with cylindrical symmetry. Then, the value of the magnetic field at different sensor positions corresponds to the magnetic field at different distances from the test sample and the magnetic intensity at the surface of the sample can be found by extrapolation. The output voltages from the Hall sensors and integrator are read by an A/D converter implemented on a data acquisition board CYDAS1600, which is controlled by a graphical programming language called DASYLAB, suitable for the development of applications such as the monitoring of the magnetizing process and generation of hysteresis curves. Magnetic properties for each specimen were determined from the hysteresis curves.

3. Results and Discussion

3.1 Magnetic Properties and Metallurgical Variables

The magnetic properties were obtained from hysteresis curves generated with the EM sensor. Figure 6 is a schematic illustrating how these properties were obtained. Table 3 presents the values for the saturated magnetic flux density, coercivity, and retentivity, as well as corresponding 95% confidence limits. The values attained in this investigation are consistent with those reported in the literature (Ref 14-20).

The magnetic saturations and coercivities were plotted as a function of the carbon content, as shown in Fig. 7. It is observed, that magnetic saturation decreased with increase in carbon content (Fig. 7a); the highest magnetic saturation reading was obtained for the hot-rolled AISI 1010 steel, and the lowest for the stress-proof AISI 1045-High Mn steel. This magnetic response is expected since the increase in carbon content causes a decrease in ferromagnetic ferrite and an increase of pearlite, particularly nonmagnetic iron carbide or cementite. The difference in magnetic saturation between the AISI 1045 and stress-proof AISI 1045-High Mn, can be attributed to the work hardening remaining in the latter sample in the presence of dislocations, as well as to the presence of sulfide inclusions (Fig. 3d). All these obstacles will cause lower induced magnetic saturation values.

On the other hand, when correlating coercivity with carbon content in the steels, the tendency was opposite (Fig. 7b), but it was also expected. Coercivity represents the intensity of the applied magnetic field required to reduce the magnetization of that material to zero. AISI 1010 and 1018 steels, Fig. 7a, showed the highest magnetic saturation measurements, because of their quick and favorable response to the applied magnetic field due to the presence of larger amounts of the magnetically soft ferrite; hence, both specimens are expected to require lower applied magnetic fields, and hence lower coercivities, to eliminate the magnetization of the steel. The steels, AISI 1045 and AISI 1045-High Mn/stress-proof, are anticipated to have higher coercivities due to the obstacles imparted by the larger volume fraction of iron carbide and lesser amounts of ferrite, as well as due to the presence of sulfides and dislocations that will pin the wall domains and thus make the demagnetization of these steels more difficult.

Better correlations between magnetic properties and microstructure were obtained when the magnetic saturations and coercivities were plotted as a function of ferrite content and ASTM grain size for the different steels (Fig. 8 and 9). As the content of the magnetically soft phase ferrite increases, the saturated magnetic induction in the steel increases and the coercivities decrease. The highest ferrite content and corresponding largest magnetic saturated induction and lowest coercivity were found in the hot-rolled AISI 1010 steel; while the stress-proof AISI 1045-High Mn steel had the lowest ferrite content. Larger amounts of pearlite, and hence iron carbide, increase the coercivity and decreases the saturated magnetic

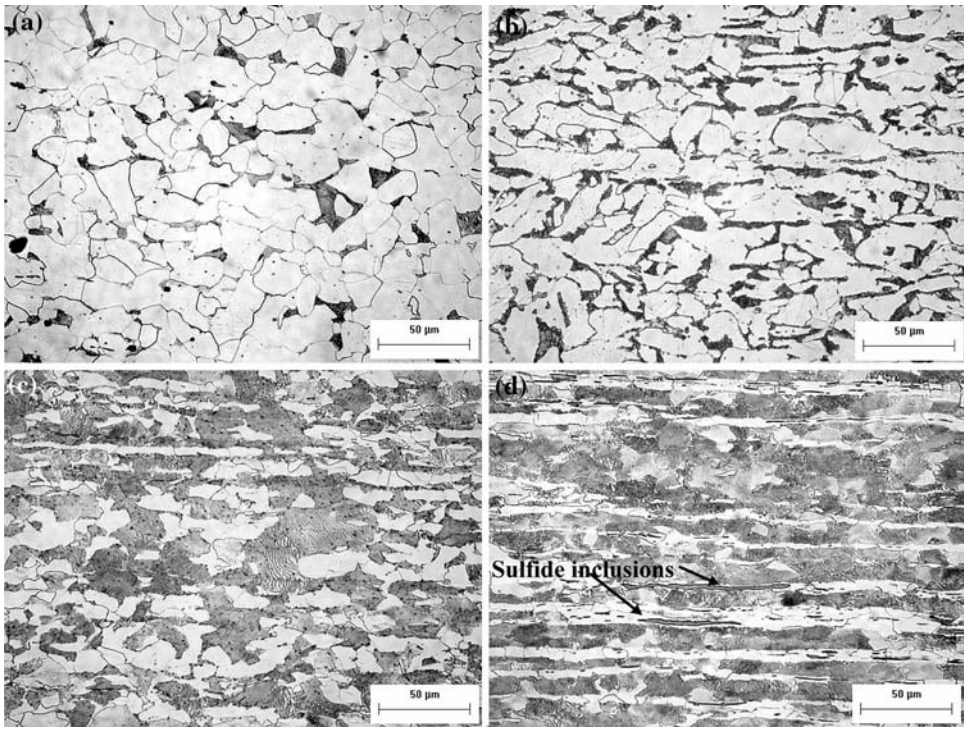

Fig. 3 Microstructures of steels: (a) Hot-rolled AISI 1010, (b) AISI 1018, (c) AISI 1045, and (d) AISI 1045-High Mn/stress-proof

Fig. 4 Appearance of AISI 1045 steels rods that were machined

induction because domain wall motion is restricted by the lamellar carbide.

The relationship between magnetic properties and grain size for all four steels establishes that the magnetic saturation declines with decrease in grain size, while the coercivity increases with

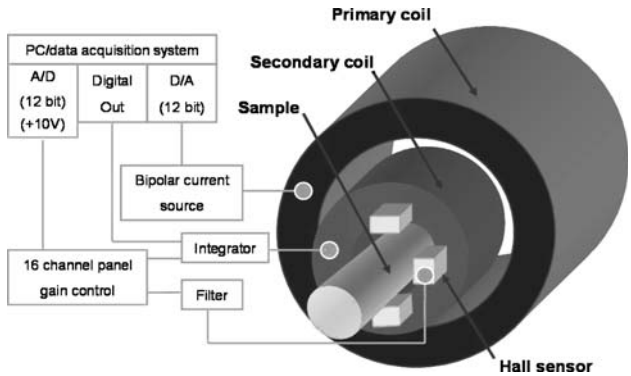

Fig. 5 Schematic of the electromagnetic sensor and measuring system

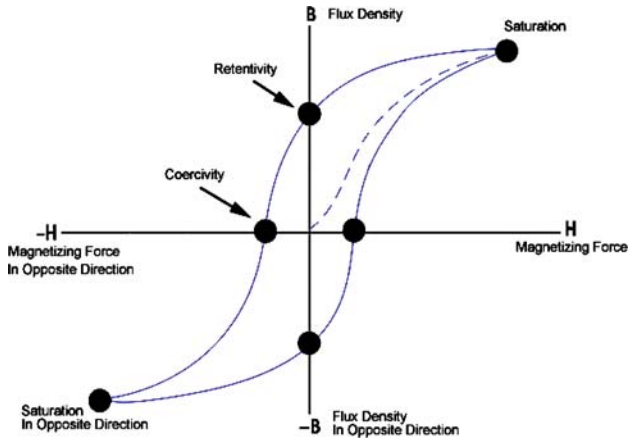

Fig. 6 Schematic of a typical hystheresis curve that illustrates the magnetic properties

Table 3 Magnetic properties for the studied steels

Steel	Magnetic property					
	Saturation, T	95% CL	Coercivity, A/m	95% CL	Retentivity, T	95% CL
AISI 1010-hot-rolled	2.0927	0.0036	685.02	5.92	0.8517	0.0005
AISI 1018	2.0786	0.0048	769.51	29.44	1.1331	0.0254
AISI 1045	2.0037	0.0027	1183.96	26.96	1.0233	0.0077
Stress-proof AISI 1045-High Mn	1.9414	0.0015	1252.32	9.56	1.2369	0.0007

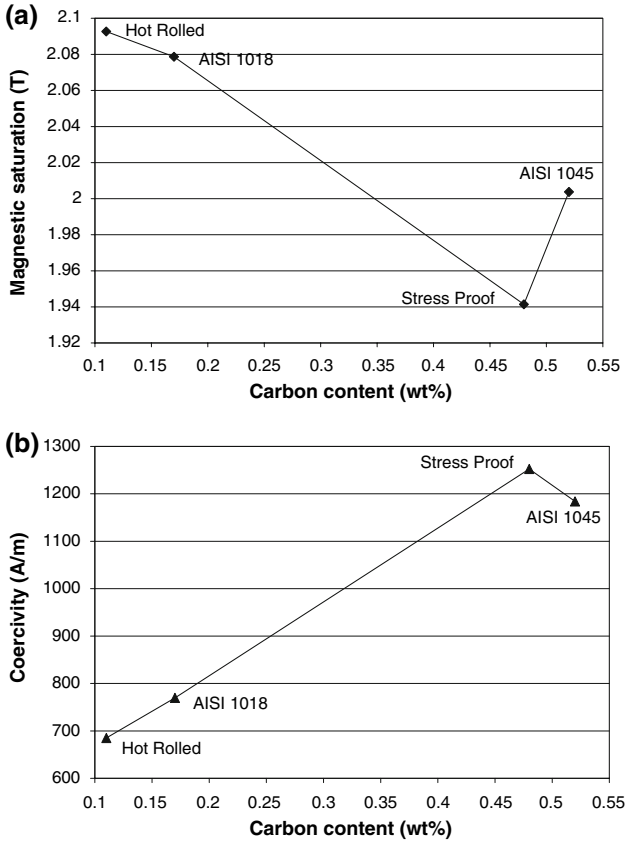

Fig. 7 Magnetic saturation (a) and coercivity (b) vs. carbon content

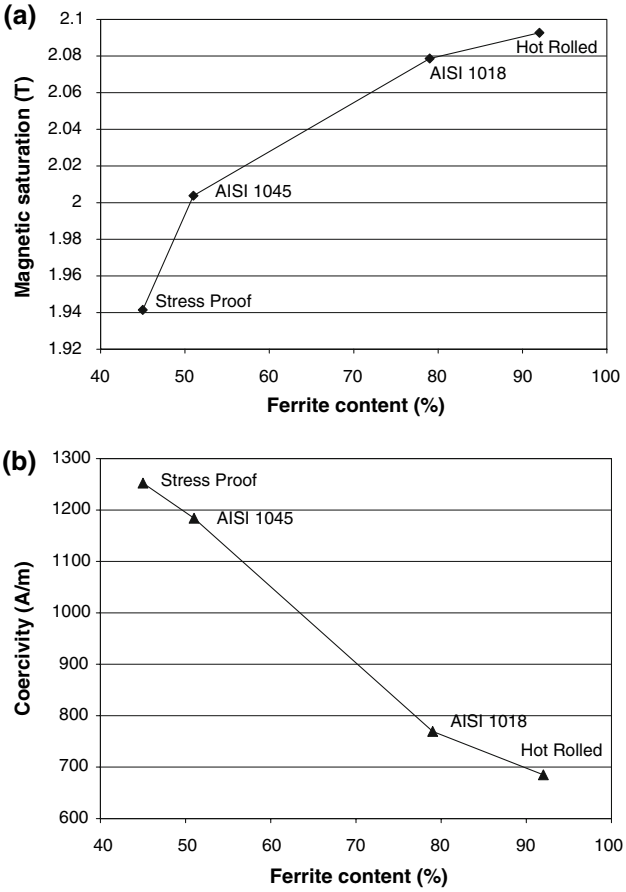

Fig. 8 Magnetic saturation (a) and coercivity (b) vs. ferrite content

grain size reduction (Fig. 9). The stress-proof AISI 1045-High Mn steel had the smallest grain structure and correspondingly the lowest magnetic saturation and highest coercivity. This implies that the grain boundaries slow down or reduce the magnetic domain walls most compared to the other steels in this study. It is speculated that grain boundaries provide obstacles to the movement of domain walls during magnetization.

The grain size is associated to the amount of cold work in the steel, which also causes a systematic variation in magnetic properties (Ref 16, 17). The degree of cold work is the highest in the stress-proof steel and the lowest in the hot-rolled. Domain wall pining becomes stronger as the dislocation density increases during cold work, producing the highest coercivity and the lowest magnetic induction in the AISI 1045-High Mn/stress-proof steel. A higher dislocation density is expected in this latter steel because of its strained condition compared to the AISI 1045 steel.

Hardness is a mechanical property in materials that encompasses chemical composition and microstructure in terms of phase distribution and grain sizes. The magnetic measurements of the steels in this study have been correlated with the hardness; as it was expected the saturated magnetic induction decreased with hardness, while the coercivity increased with hardness as observed in Fig. 10. The increase in the amount of pearlite due to the higher carbon, the decrease in grain size, and the remaining strain of the steels as a result of deformation, contributed to produce a material less responsive to magnetization on application of a magnetic field. Furthermore, as the materials became magnetized, it took a larger applied magnetic field (large coercivity, Fig. 10b) to reduce the induced magnetization to zero for the harder steels (AISI 1045-High Mn/stress-proof and the AISI 1045) compared to the softer ones (AISI 1010 and 1018 steels) that show lower coercivities.

No correlations could be found between retentivity and microstructural features and hardness for these steels. Retentivity has been reported to be mostly affected by carbide

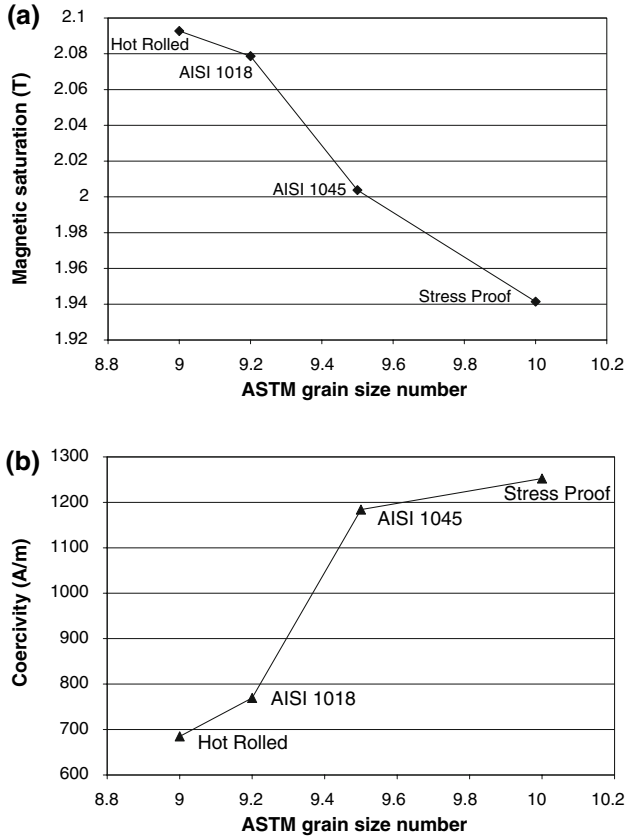

Fig. 9 Magnetic saturation (a) and coercivity (b) vs. ASTM grain size number

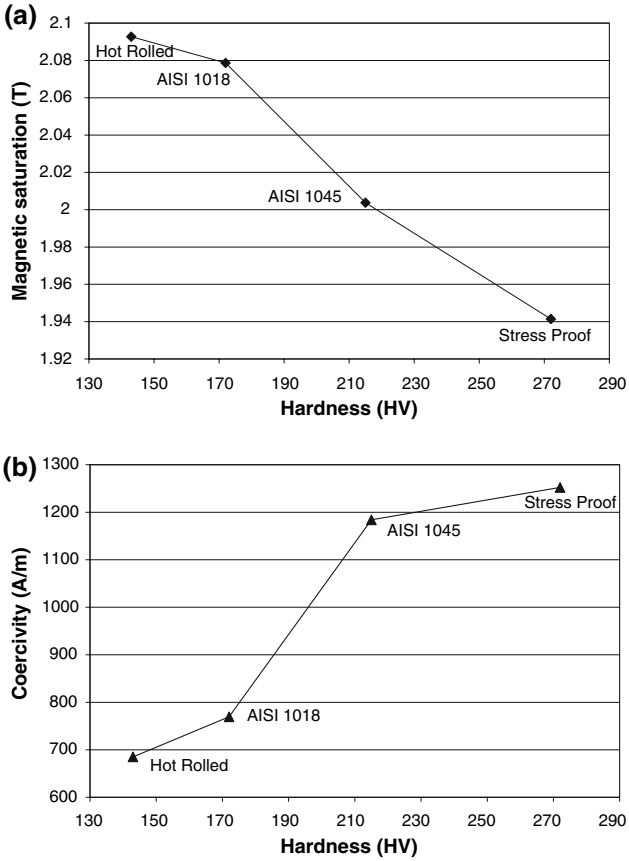

Fig. 10 Magnetic saturation (a) and coercivity (b) vs. Vickers hardness

morphology; in this investigation, all the steels exhibit the same lamellar carbide morphology, except the amounts of iron carbide increased with the carbon content of the steel. Figure 11 reflects this lack of correlation.

3.2 Impact of Specimen Diameter Reductions on Magnetic Measurements

The objective in this portion of the investigation was to determine if this sensor could be expanded to the detection of uniform corrosion in steels considering a homogeneous reduction of the diameter of the steel due to surface degradation. As pointed out above, the diameter reductions were carried out by machining systematically each of the steel specimens and carrying out measurement at each reduction. The reduction in cross-section area of the steel rods is accompanied by a mass loss, which was normalized according to the length of the machined zone (Fig. 4). The results are presented in Table 4.

Figure 12 shows the hysteresis curves obtained for each level of reduction for all steels. The 0% reduction corresponds to the sample without any reduction in area. Then, as the diameter of the steel was reduced it is observed in Fig. 12 that the saturated magnetic flux density decreased; this is contrary to what it would be expected. This occurs because in the calculations to convert the output voltage into magnetic flux density B, the cross-section area was assumed constant in all cases and equal to 122.7 mm^2, the cross-section area of samples without any reduction in area. In addition, as the diameter of the sample is reduced, the air gap between the sensing coil and the rod increases, producing localized magnetic fields opposite to the direction of the applied

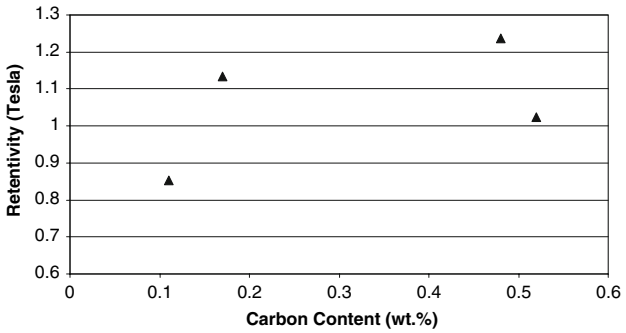

Fig. 11 Retentivity vs. carbon content plot for the steels studied in this investigation

Table 4 Normalized mass loss for all steel samples due to the reduction in diameter

Reduction in cross-section area, %	Normalized mass loss, g/cm^2
5	0.1221
10	0.2443
15	0.3665

magnetic field. Consequently, demagnetizing forces will develop causing flux leakage, which reduces the magnetic flux in the rods as their cross-section areas are reduced. This

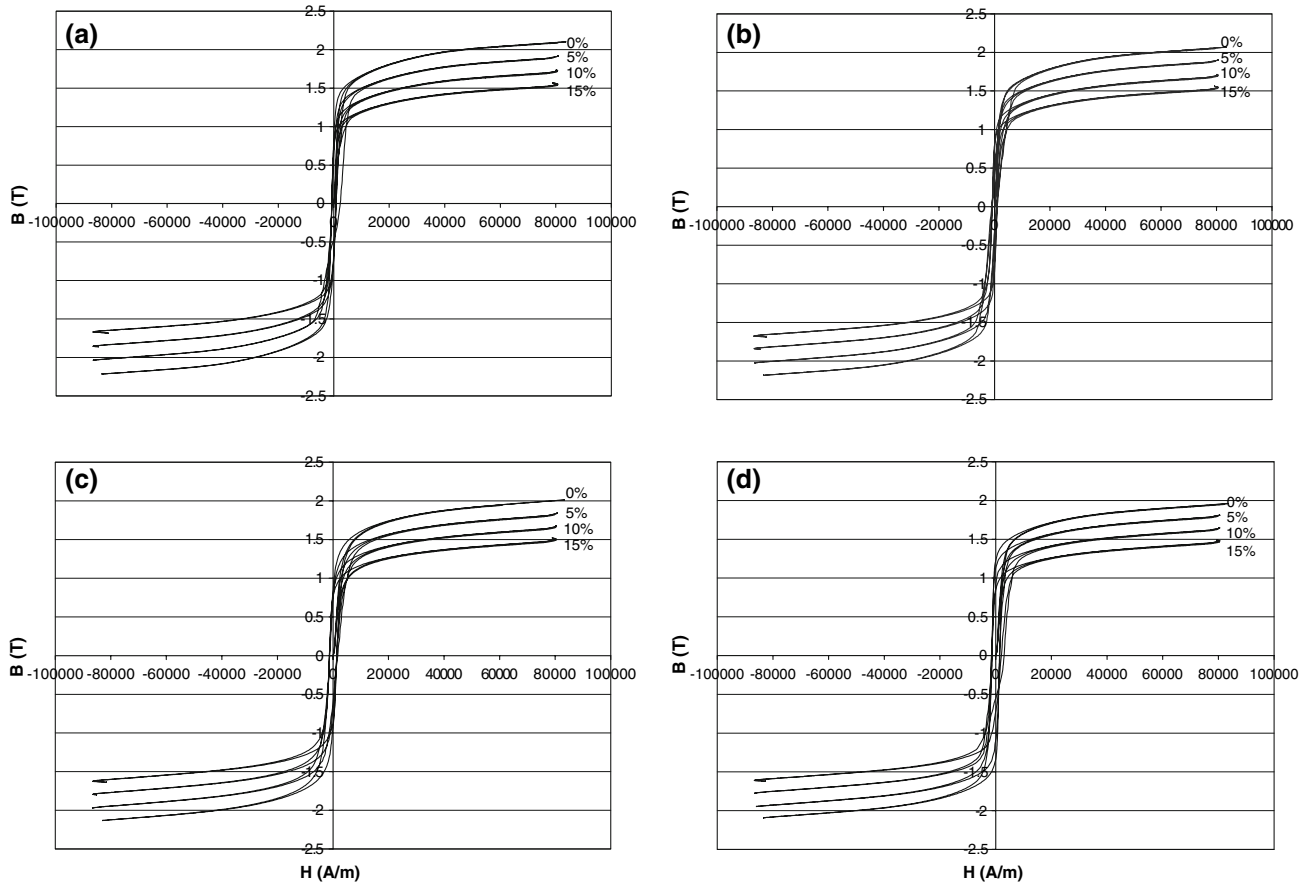

Fig. 12 Hysteresis curves for hot-rolled (a), AISI 1018 (b), AISI 1045 (c), and stress-proof (d) steels at different levels of reduction in cross-section area

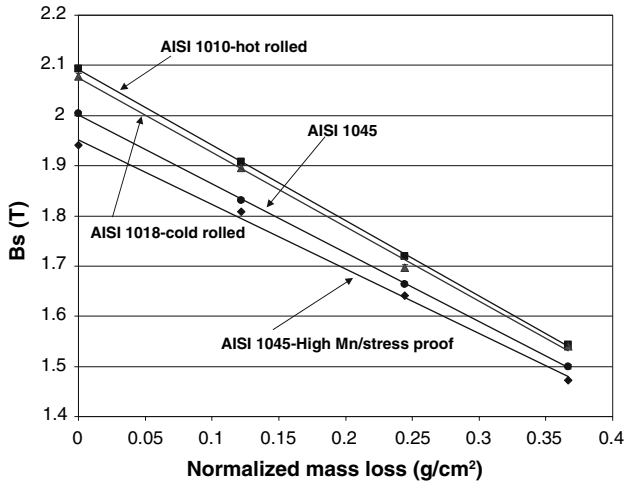

Fig. 13 Magnetic saturation vs. normalized mass loss for the machined samples

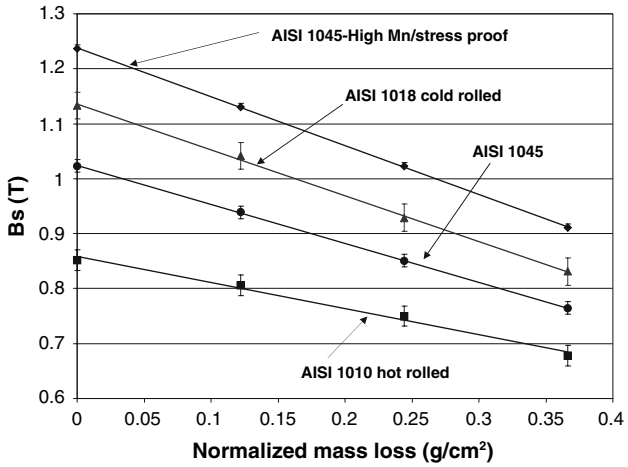

Fig. 14 Retentivity vs. normalized mass loss for the machined samples

assumption allows us to establish a correlation for cases when the reduction in area cannot be accurately measured, as is in the case of materials degradation mechanisms. Looking at the hysteresis curves for the AISI 1010-hot-rolled steel rod plotted in Fig. 12(a), the magnitude of the saturated magnetic flux density (B_s) drops from a value of 2.09 T for the original diameter of 12.5 mm, or zero mass loss, to approximately 1.55 T at 15% cross-sectional area reduction (0.37 g/cm^2 mass loss) following a linear relationship. A similar trend was observed for the AISI 1018, AISI 1045, and AISI 1045-High Mn/stress-proof steels.

The saturated magnetic flux densities B_s corresponding to the different types of steel rods were plotted as a function of the normalized mass loss as shown in Fig. 13. As expected, the magnetic flux densities for the four types of steel rods are different; the AISI 1010-hot-rolled steel shows consistently the highest values compared to the AISI 1018, AISI 1045, and AISI 1045-high Mn/stress-proof steel rods. The magnetic retentivity, B_r, was also plotted as a function of the normalized mass loss for all steel rods, as shown in Fig. 14. A linear relationship was observed again where the retentivity decreased with cross-section area reduction or mass loss. Based on calculated 95% confidence limits it was determined that magnetic flux saturation was more sensitive to the small systematic diameter reductions. Therefore, variations in cross-section area of steels can be predicted based on saturated magnetic flux density measured by the EM sensor. A specific application was found in the quantification of small mass losses due to early corrosion in structural steels reported in our previous publications (Ref 21, 22).

4. Conclusions

1. It was observed that the carbon content of the steels affected the magnetic behavior of the steels. It was established that the increase in the amount of iron carbide (cementite) of the steels reduced their magnetization potential.
2. The induced magnetic saturation and coercivity measured with the EM sensor can be reliably correlated to percent of ferrite, grain size, and hardness of the steel.
3. The reductions in the cross-section area of the steel rods caused a decrease in the induced saturated flux, as well as in the magnetic retentivity. Both quantities had a linear correlation with the mass loss.
4. It was established that electromagnetic sensor can be confidently used to identify microstructure features and estimate variations in cross-section area in structural steels.

Acknowledgment

The authors wish to express their gratitude to the National Science Foundation (Grant # NSF CMS-0434516) for the support for this investigation.

References

1. M.B. Mesina, T.P.R. de Jong, and W.L. Dalminj, Scrap Stainless Steel Detection using a Pulsed Electromagnetic Field, *Int. J. Miner. Proces.*, 2005, **76**, p 21–31
2. R.J. Haldane, W. Yin, M. Strangwood, A.J. Peyton, and C.L. Davis, Multi-Frequency Electromagnetic Sensor Measurement of Ferrite/Austenite Phase Fraction – Experiment and Theory, *Scripta Mater.*, 2006, **54**, p 1761–1765
3. M.Ph. Papaelias, M. Strangwood, A.J. Peyton, and C.L. Davis, Effect of Microstructural Variations on Smart Inductive Sensor Measurements of Phase Transformation is Steel, *Scripta Mater.*, 2004, **51**, p 379–383
4. K. Mohri, T. Uchiyama, L.P. Shen, C.M. Cai, and L.V. Panina, Amorphous Wire and CMOS IC-based sensitive Micro-magnetic Sensors for Intelligent Measurements and Controls, *J. Magn. Magn. Mater.*, 2002, **249**, p 351–356
5. R. Taylor, An Online Grain Size Measuring System for Electrical Steel Production, *J. Magn. Magn. Mater.*, 1992, **112**, p 95–98
6. J. Degauque, B. Astie, J.L. Porteseil, and R. Vergne, Influence of the Grain Size on the Magnetic and Magnetomechanical Properties of High-Purity Iron, *J. Magn. Magn. Mater.*, 1982, **26**, p 261–263
7. J. Anglada-Rivera, L.R. Padovese, and J. Capo-Sanchez, Magnetic Barkhausen Noise and Hysteresis Loop in Commercial Carbon Steel: Influence of Applied Stress and Grain Size, *J. Magn. Magn. Mater.*, 2001, **231**, p 299–306
8. B.K. Tanner, J.A. Szpunar, S.N. Willcock, L.L. Morgan, and P.A. Mundell, Magnetic and Metallurgical Properties of High-Tensile Steels, *J. Mater. Sci.*, 1988, **23**, p 4534–4540
9. M. Yoshino, H. Tanabe, T. Sakamoto, N. Suzuki, and Y. Yaji, Nondestructive Measurement of Grain Size in Steel Plates by Using Magnetic Coercive Force, *Mater. Sci. Forum*, 1996, **210–213**, p 45–54
10. S. Koontz, "Magnetoelastic Measurement of Permeability for Non-Destructive Testing Force Monitoring in Prestressed Cables," MS Thesis, Department of Civil and Materials Engineering, University of Illinois at Chicago, 2000
11. O. Hovorka, "Measurement of Hysteresis Curves for Computational Simulation of Magnetoelastic Stress Sensors," MS Thesis, Department of Civil and Materials Engineering, University of Illinois at Chicago, 2002
12. V. Singh, "Measurement of Corrosion of Steel Reinforcement by Electromagnetic Non-Destructive Evaluation Technique," PhD Thesis, Department of Civil and Materials Engineering, University of Illinois at Chicago, 2003
13. F. Rumiche, J.E. Indacochea, and M.L. Wang, Detection and Monitoring of Corrosion in Structural Carbon Steels using Electromagnetic Sensors, submitted to the Engineering Materials and Technology Journal. Recommended for publication and under 2nd review, October 2007
14. J. Anglada-Rivera, L.R. Padovese, and J. Capo-Sanchez, Magnetic Barkhausen Noise and Hysteresis Loop in Commercial Carbon Steel: Influence of Applied Stress and Grain Size, *J. Magn. Magn. Mater.*, 2001, **231**, p 299–306
15. O. Saquet, J. Chicois, and A. Vincent, Barkhausen Noise from Plain Carbon Steels: Analysis of the Influence of the Microstructure, *Mater. Sci. Eng.*, 1999, **A269**, p 73–82
16. D.C. Jiles, The Effect of Compressive Plastic Deformation on the Magnetic Properties of AISI 4130 Steels with Various Microstructures, *J. Phys. D: Appl. Phys.*, 1988, **21**, p 1196–1204
17. A.J. Birkett, W.D. Corner, B.K. Tanner, and S.M. Thompson, Influence of Plastic Deformation on Barkhausen Power Spectra in Steels, *J. Phys. D: Appl. Phys.*, 1989, **22**, p 1240–1242
18. D.C. Jiles, Magnetic Properties and Microstructure of AISI 1000 series Carbon Steels, *J. Phys. D: Appl. Phys.*, 1988, **21**, p 1186–1195
19. J.M. Lopez, J. Degauque, B. Astie, J. Garigue, and J.P. Redoules, "Correlation entre Differents Etats de la Precipitation de la Cementite et les Proprietes Magnetiques et Magnetomecaniques d'Alliages fer Pur-Carbone," Memoires et Etudes Scientifiques Revue de Metallurgie, 1985
20. A. Polar, J.E. Indacochea, M.L. Wang, V. Singh, and G. Lloyd, Measurement and Microstructural Evaluation of Creep-Induced Changes in Magnetic Properties of a 410 Stainless Steel, *ASME J. Eng. Mater. Technol.*, 2004, **126**, p 392–397
21. F. Rumiche, "Early Corrosion Detection and Monitoring in Structural Steels using Magnetic Sensors," MS Thesis, Department of Civil and Materials Engineering, University of Illinois at Chicago, 2005
22. F. Rumiche, J.E. Indacochea, and M.L. Wang, Early Corrosion Detection in Structural Carbon Steels using Electromagnetic Sensors, *Proceedings for Smart Structures and Materials 2006: Sensors and Smart Structures Technologies for Civil, Mechanical and Aerospace Systems*, Vol. 6174, SPIE, February 2006 (San Diego, CA, USA), 2006